Materials Origins of Decoherence in Superconducting Qubits

Robert McDermott

(Invited Paper)

***Abstract*—Superconducting integrated circuits incorporating Josephson junctions are an attractive candidate for scalable quantum information processing in the solid state. The strong nonlinearity of the Josephson effect enables one to tailor an anharmonic potential and thus to realize an artificial quantum two-level system ("qubit") from a macroscopic superconducting circuit. Josephson qubits can be made to interact strongly and controllably, and it should be straightforward to fabricate circuits incorporating hundreds or even thousands of Josephson qubits using standard thin-film processing techniques. Work over the last several years has shown that qubit performance is limited by spurious coupling of the qubit to microscopic defect states in the materials that are used to implement the circuit. Here we discuss the materials origins of dissipation and dephasing in superconducting qubits. A deeper understanding of the underlying materials physics that governs decoherence in superconducting quantum circuits will guide the search for improved, low-noise materials and fuel continued progress in the field of superconducting quantum computing.**

***Index Terms*—Superconducting device noise, superconducting integrated circuits, superconducting materials.**

I. Introduction

THERE has been tremendous progress recently in efforts to implement quantum bits ("qubits") using superconducting integrated circuits incorporating Josephson junctions [1]–[4]. These circuits can be thought of as artificial atoms, with energy levels that can be tuned over a broad range by appropriate variation of the circuit design parameters and bias. In contrast to Nature-given quantum systems such as atoms or nuclear spins, superconducting qubit circuits can be made to interact strongly with one another simply by connecting the circuits with wires and linear circuit elements such as capacitors and inductors. In principle, then, it should be straightforward to scale up to circuits comprising many qubits, once the single qubit circuits have achieved high-fidelity operation. However, superconducting quantum circuits also couple strongly to spurious sources of dissipation and dephasing in the environment, and these act to destroy the quantum coherence of the qubit state. Work over the last several years has shown that a dominant source of decoherence in superconducting qubits is microscopic two-level state (TLS) defects in the amorphous materials that are used to implement the qubit circuit. Here we focus on the underlying materials physics that governs decoherence in superconducting circuits, and outline some of the approaches that are currently being pursued to realize qubits with improved coherence properties.

This review is organized as follows. In Section II, we provide a brief introduction to the operation of Josephson qubit circuits and we discuss in general terms dissipation and dephasing of a quantum two-level system. In Section III, we describe the basic physics of charged TLS defects in amorphous dielectric materials. In Sections IV and V, we describe how interaction of the qubit with TLS defects leads to energy relaxation and fidelity loss, respectively, and we discuss ongoing efforts to improve the crystalline quality of the qubit dielectrics. In Sections VI–VIII, we discuss qubit dephasing induced by low-frequency critical-current, charge, and flux noise, respectively. Finally, in Section IX, we highlight some open questions, and discuss potential strategies for the realization of improved qubit materials.

II. Superconducting Integrated Circuits as Qubits

The key to all superconducting qubits is the Josephson junction: a weak link separating two superconducting electrodes. In the vast majority of superconducting qubit work to date, the superconductor is sputter-deposited or evaporated aluminum or niobium, and the Josephson junction is formed by thermal oxidation of an amorphous aluminum layer to form an AlO_x tunnel barrier. As Josephson first showed, Cooper pairs can tunnel coherently through the junction [5], yielding a pair current I and voltage V across the junction that are related to the difference δ in the superconducting phase across the junction

$$\begin{aligned} I &= I_0 \sin \delta \\ V &= \frac{\Phi_0}{2\pi}\dot{\delta}. \end{aligned} \tag{1}$$

Here the critical-current I_0 is the maximum pair current that the junction can support, and $\Phi_0 = h/2e \approx 2.07 \times 10^{-15}$ Tm^2 is the magnetic flux quantum [4]. These two equations can be combined to form a single equation that describes the effective inductance L_J of the Josephson junction

$$L_J = \frac{\Phi_0}{2\pi I_0 \cos \delta}. \tag{2}$$

The Josephson inductance is highly nonlinear, due to the $\cos \delta$ term in the denominator of (2): for example, as the junction is biased with a current I_b approaching the critical-current I_0, the

Manuscript received November 17, 2008; revised December 27, 2008. First published January 20, 2009; current version published January 28, 2009. This paper was recommended by Associate Editor M. Mueck.

The author is with the Department of Physics, University of Wisconsin, Madison, WI, 53706 USA (e-mail: rfmcdermott@wisc.edu).

Color versions of one or more of the figures in this paper are available online at http://ieeexplore.ieee.org.

Digital Object Identifier 10.1109/TASC.2008.2012255

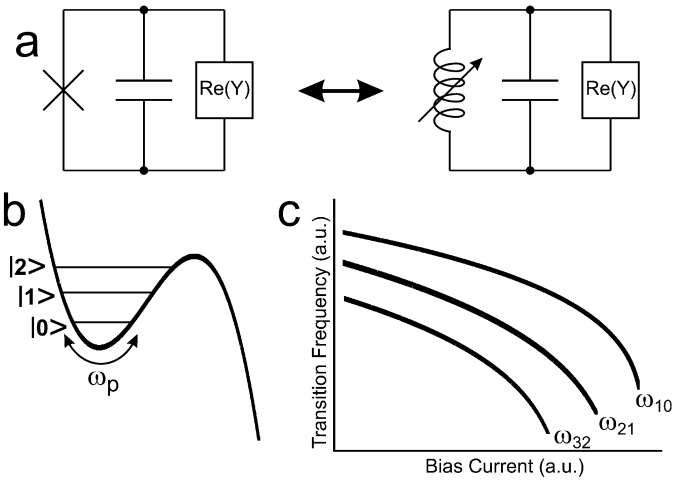

Fig. 1. (a) Josephson tunnel junction as an anharmonic LC resonator. (b) Cubic potential energy landscape $U(\delta)$ of the current-biased Josephson junction. Due to the anharmonicity of the potential, the energy levels are unequally spaced. (c) Transition frequencies versus bias for the current-biased Josephson junction.

phase difference δ across the junction approaches $\pi/2$, and the Josephson inductance diverges.

In parallel with the nonlinear Josephson inductance there is a linear self-capacitance C associated with the metal–insulator–metal structure of the tunnel barrier. The parallel combination of effective inductance and capacitance forms a plasma resonance, typically in the gigahertz range. Due to the nonlinearity of the Josephson inductance, the potential energy landscape that gives rise to the plasma resonance is anharmonic. For a junction in the quantum regime, this means that the spacings between the discrete levels in the local minima of the potential are unequal, providing the opportunity to selectively address the two lowest energy levels with resonant irradiation, and thus to implement a qubit (Fig. 1).

For the sake of concreteness, let us consider a single Josephson junction biased with a current $I_b \lesssim I_0$; this is the prototypical phase qubit [6], [7]. The potential energy landscape takes on the familiar "tilted washboard" form [8]

$$U(\delta) = \frac{-I_0\Phi_0}{2\pi}\cos\,\delta - \frac{I_b\Phi_0}{2\pi}\delta. \tag{3}$$

As I_b approaches I_0, the washboard potential can accurately be parameterized as cubic in the vicinity of the local minima [9], [10]. The junction phase is localized near $\delta = \pi/2$, where the curvature of the potential yields a classical plasma frequency ω_p given by

$$\omega_p = 2^{1/4}\left(2\pi I_0/\Phi_0 C\right)^{1/2}\left[1 - I_b/I_0\right]^{1/4}. \tag{4}$$

Due to the cubic anharmonicity, the spacings of the discrete energy levels E_n that reside in the local minima of the potential are nondegenerate. For typical parameters, one has $\omega_{10} \equiv (E_1 - E_0)/\hbar \approx 0.95\omega_p$, while $(\omega_{10} - \omega_{21})/\omega_{10}$ is of the order of a few percent [10].

Other superconducting qubits are formed by exploiting the Josephson nonlinearity in different ways. In the Josephson flux qubit, the junction is embedded in a superconducting loop that is flux-biased near degeneracy $\Phi_b \approx \Phi_0/2$ [11], [12]. In this case, the effective inductance of the junction is negative, and the potential energy landscape is quartic, with qubit states corresponding to symmetric and antisymmetric superpositions of circulating current states localized in the minima of the quartic double-well potential. The Josephson charge qubit [13] consists of a small superconducting island with capacitance C_Σ separated from a charge reservoir by a Josephson junction. The charging energy $E_C \equiv (2e)^2/2C_\Sigma$ of the island is typically larger than the Josephson energy $E_J \equiv I_0\Phi_0/2\pi$, and the qubit states correspond to zero or one excess Cooper pair on the island; in the conjugate phase representation the qubit states are delocalized Bloch states. A thorough discussion of the various superconducting qubit types can be found in [2]. When the qubit circuit is cooled to low enough temperatures and spurious coupling to external noise is suppressed, one can probe the collective quantum properties of these macroscopic artificial atoms. External control parameters (current, flux, or charge, depending on the qubit flavor) are adjusted in order to tune the energy separation between qubit levels, and resonant microwaves are used to drive coherent transitions between the qubit states [6], [14], [15].

We now turn to the issue of qubit coherence. Decoherence is described by two phenomenological parameters T_1 and T_2 that govern longitudinal and transverse relaxation of the qubit state, respectively [16]. At low temperatures $T \ll \hbar\omega_{10}/k_B$, stimulated transitions between the qubit levels due to thermal photons are greatly suppressed, and longitudinal relaxation proceeds via spontaneous decay of the qubit $|1\rangle$ state. This decay rate is intimately connected to the real part of the admittance shunting the qubit junction [10], [17]

$$\frac{1}{T_1} = \frac{\mathrm{Re}\;Y(\omega_{10})}{C}. \tag{5}$$

Here, $\mathrm{Re}\;Y(\omega_{10})$ has contributions from several parallel dissipation channels. First, the electrical leads that are connected to the qubit to perform low-frequency biasing, high-frequency control, and readout all contribute to the spontaneous emission from the qubit. However, the effective impedance seen by the qubit as it looks into the control and readout lines can be made quite large by appropriate use of broadband inductive and capacitive impedance transformers. An alternative approach is to couple the qubit to the outside world via a resonant cavity or transmission line resonator [18]–[20], which has the effect of suppressing qubit spontaneous emission at frequencies far removed from the cavity resonance, a phenomenon analogous to the Purcell effect in atomic physics. Thus, by appropriate circuit design, one can effectively suppress dissipation induced by the electrical leads.

A more serious source of dissipation is microscopic materials defects inherent in the amorphous thin films that are used to implement the qubit. While the energy gap of the superconductor provides a natural barrier against dissipation, charged TLS defects in the amorphous dielectrics of the circuit provide a high density of low-energy states to which the qubit can couple. Thus, it is not the nonlinear Josephson inductance—the key to the realization of a superconducting qubit—that limits energy relaxation times; rather, it is the "simple" linear self-capacitance of the qubit. In Section III, we summarize the basic physics of charged TLS in dielectric films, and in Sections IV and V, we describe qubit energy relaxation and fidelity loss induced by dielectric TLS.

Transverse relaxation of the qubit has contributions from spontaneous decay and from pure dephasing

$$\frac{1}{T_2} = \frac{1}{2T_1} + \frac{1}{T_\phi} \tag{6}$$

where the pure dephasing rate $1/T_\phi$ is governed by low-frequency fluctuations in the control parameters λ that determine the energy separation between the qubit states [10], [17]. In the case of a low-frequency spectrum $S_\lambda(\omega)$ of bias fluctuations that is white, one can show that the dephasing rate is given by

$$\frac{1}{T_\phi} = \pi \left(\frac{\partial \omega_{10}}{\partial \lambda}\right)^2 S_\lambda(\omega = 0). \tag{7}$$

For most practical cases of interest, however, the spectral density of fluctuations in the qubit control parameter is singular at low frequencies, with a spectrum that scales inversely with frequency: $S_\lambda(\omega) = A/\omega$. This so-called $1/f$ noise is typically understood to arise from the fluctuations of an ensemble of underlying TLS with a broad distribution of characteristic relaxation times [21]–[23]. In the presence of $1/f$ bias noise, a coherent superposition of the qubit states $|0\rangle$ and $|1\rangle$ decays in time with a Gaussian envelope described by [10], [17]

$$f(t) \approx \exp\left[-\left(\frac{\partial \omega_{10}}{\partial \lambda}\right)^2 A \ln\left(\frac{1}{\omega_m t}\right) t^2\right]. \tag{8}$$

While the deleterious effects of low-frequency bias noise can be mitigated by the use of spin-echo-type refocusing techniques [16], the effectiveness of refocusing pulses is limited unless dephasing times are much longer than gate times, a situation which is typically not realized. For this reason, it is desirable to develop a deep understanding of all potential sources of low-frequency bias noise in superconducting circuits, in order to point the direction to the realization of qubit materials and circuit designs with improved noise properties. A detailed discussion of qubit dephasing induced by $1/f$ critical-current, charge, and flux noise is given in Sections VI–VIII.

III. TLS Defects in Amorphous Materials

Low-energy TLS defects are widely believed to account for many of the anomalous properties of glasses at low temperature, including a specific heat that varies linearly in temperature T, a T^2 dependence of the thermal conductivity, and a strong enhancement of acoustic and dielectric absorption [24]–[27]. Moreover, an ensemble of TLS defects gives rise to the low-frequency $1/f$ noise that is universally observed in electronic devices from semiconducting field-effect transistors to superconducting quantum interference devices (SQUIDs) [21], [28], and which is the dominant source of dephasing in superconducting qubits [10], [23].

In the so-called "tunneling model" of TLS defects [26], an atomic-scale materials defect resides in a potential energy landscape that displays two local minima separated by a small energy difference, and between which the defect can hop via either thermal activation or quantum mechanical tunneling (Fig. 2). For a sufficiently large tunneling matrix element, the eigenstates are appropriate superpositions of wavefunctions localized in the two potential minima. We consider a TLS defect that can exist in one of two configurational states $|L\rangle$ and $|R\rangle$, corresponding to local minima in the double-well potential energy landscape. The energy separation between these configurational states is Δ; the tunneling matrix element Δ_0 connects the configurational states. The Hamiltonian for the TLS is thus

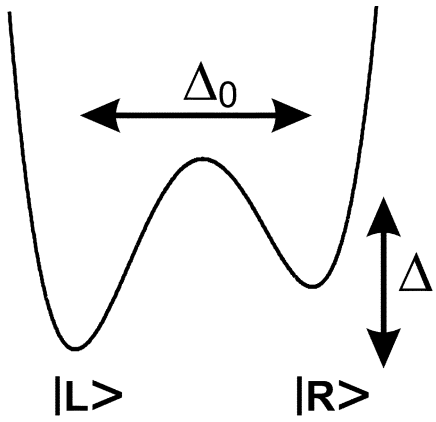

Fig. 2. Schematic of TLS double-well potential, showing asymmetry Δ and tunneling energy Δ_0 for the localized configurational states $|L\rangle$ and $|R\rangle$.

$$H_{\rm TLS} = \frac{1}{2}\begin{pmatrix} \Delta & \Delta_0 \\ \Delta_0 & -\Delta \end{pmatrix}. \tag{9}$$

The TLS eigenstates are then

$$\begin{aligned} |g\rangle &= \sin(\theta/2)\,|L\rangle + \cos(\theta/2)\,|R\rangle \\ |e\rangle &= \cos(\theta/2)\,|L\rangle - \sin(\theta/2)\,|R\rangle \end{aligned} \tag{10}$$

where $\theta = \arctan(\Delta_0/\Delta)$; these states are separated in energy by $\epsilon \equiv (\Delta^2 + \Delta_0^2)^{1/2}$.

Typically, the distribution of TLS bias energies is understood to be uniform, while the distribution of tunneling matrix elements is log-uniform, due to the exponential dependence of tunneling on barrier height

$$P(\Delta, \Delta_0) \propto \frac{1}{\Delta_0}. \tag{11}$$

Performing a change of variables from (Δ, Δ_0) to $(\epsilon, \sin\theta)$, we have

$$P(\epsilon, \sin\theta) \propto \frac{1}{\cos\theta \sin\theta}. \tag{12}$$

Thus, according to the standard tunneling model of TLS, the density of defect states is independent of energy ϵ.

If there is a charge associated with the defect state, there will be an electric dipole moment $\mathbf{d}$ corresponding to the configurational change that takes the defect from $|L\rangle$ to $|R\rangle$. For a typical TLS defect in an amorphous dielectric, we expect an electric dipole moment of order 1 Debye (roughly 1 electron charge times the Bohr radius). The interaction between the TLS dipole and an applied electric field $\mathbf{E}$ is governed by the Hamiltonian

$$\begin{aligned} H_{\rm int} &= -\,\mathbf{d}\cdot\mathbf{E} \\ &= -\,d\;E\;\cos\eta\,(|L\rangle\langle L| - |R\rangle\langle R|) \end{aligned} \tag{13}$$

where the angle η accounts for the relative orientation of the TLS dipole moment and the applied field. Transforming to the TLS eigenbasis, we find

$$\begin{aligned} H_{\rm int} &= -\,d\,E\cos\eta\,[\cos\theta(|E\rangle\langle e| - |g\rangle\langle g|) \\ &\qquad + \sin\theta(|e\rangle\langle g| + |g\rangle\langle e|)] \\ &= -\,d\,E\cos\eta\begin{pmatrix}\cos\theta & \sin\theta \\ \sin\theta & -\cos\theta\end{pmatrix} \\ &= -\,d\,E\cos\eta\,(\cos\theta\;\sigma_z + \sin\theta\;\sigma_x) \end{aligned} \tag{14}$$

where $\hat{\sigma}$ are the usual Pauli matrices in the TLS eigenbasis. For defect energies larger than k_BT, the TLS defects behave like a "spin bath" in the quantum regime, and the spin physics gives rise to such unusual properties as enhanced dielectric loss at low temperature and low microwave drive power [29]; on the other hand, defects with energies less than k_BT produce low-frequency charge and dielectric noise [30]–[32]. The quantum TLS contribute to qubit energy relaxation, while the thermal TLS contribute to qubit dephasing.

IV. Dissipation From Materials Defects

Just as a resonant magnetic field can induce transitions in a system of spins immersed in a strong static magnetic field, resonant electric fields can couple to TLS with an electric dipole moment, inducing transitions and dissipation. We consider TLS states resonating at frequency ω_T and subjected to a transverse electric field with amplitude E at frequency ω. The externally applied resonant field results in upward and downward transitions between the TLS states at a rate $\Gamma_{\rm ext}$; at the same time, spontaneous emission drives the TLS from the state $|e\rangle$ to $|g\rangle$ at a rate $1/\tau_1$. The power per unit volume absorbed from the driving field by the TLS is given by

$$dP_a = \langle n\rangle\Gamma_{\rm ext}\,\hbar\omega_T\,\rho\,d\epsilon \tag{15}$$

where $\langle n\rangle \equiv \langle n_g\rangle - \langle n_e\rangle$ is the population difference of the TLS ground and excited states, and where ρ is the TLS energy density of states per unit volume. Since the transitions induced by the external drive field are incoherent, the rate $\Gamma_{\rm ext}$ is proportional to the square of the driving field; in fact, a simple analysis from Fermi's Golden Rule shows that the transition rate is given by

$$\Gamma_{\rm ext}(\Omega) = 2\omega_R^2\frac{\tau_2}{1+\Omega^2\tau_2^2} \tag{16}$$

where τ_2 is the TLS transverse relaxation time [4], $\Omega \equiv \omega_T - \omega$ is the detuning of the TLS frequency from the driving frequency, and where the Rabi frequency ω_R is given by

$$\omega_R = \frac{Ed}{2\hbar}\cos\eta\sin\theta. \tag{17}$$

In the presence of both thermal and externally driven transitions, we have

$$\langle n\rangle = \frac{\tanh(\hbar\omega_T/2k_BT)}{1+2\Gamma_{\rm ext}\tau_1} \tag{18}$$

where in general τ_1 is temperature-dependent. To compute the total power absorbed by the TLS system, we integrate over the TLS distribution (12) and over all angular orientations η. We find

$$P_a = \frac{\pi}{6}\frac{\tanh(\hbar\omega_T/2k_BT)}{\sqrt{1+\omega_R^2\tau_1\tau_2}}\,\rho d^2\,\omega_T\,E^2. \tag{19}$$

The loss tangent $\tan\delta$ of the dielectric is defined as the ratio of the energy absorbed per unit volume per radian of oscillation to the maximum energy density of the electric field

$$\tan\delta = \frac{2P_a}{\omega\epsilon_r\epsilon_0E^2}. \tag{20}$$

The dielectric loss induced by the TLS is thus expressed as

$$\tan\delta = \frac{\pi}{3}\frac{\rho d^2}{\epsilon_0\epsilon_r}\frac{\tanh(\hbar\omega_T/2k_BT)}{\sqrt{1+\omega_R^2\tau_1\tau_2}}. \tag{21}$$

Note that the loss tangent of the amorphous dielectric decreases due to population of the TLS excited state: as thermal or external microwave transitions saturate the TLS, the dielectric becomes transparent to resonant irradiation, and the loss decreases. In the case of qubit experiments, however, one typically works at a temperature around 20 mK and at extremely low microwave drive powers, corresponding to one microwave photon loaded into the anharmonic qubit resonance. In this case, we are interested in the *intrinsic* low-temperature ($k_BT \ll \hbar\omega_{\rm TLS}$), low-power ($\omega_R = 0$) loss tangent of the amorphous dielectric

$$\tan\delta_i = \frac{\pi}{3}\frac{\rho d^2}{\epsilon_0\epsilon_r}. \tag{22}$$

For the parameters $d = 1$ Debye, $\rho = 10^{46}$ J$^{-1}\cdot$m^{-3}, and $\epsilon_r = 4$ (characteristic of amorphous SiO_2 [26]), we find a large intrinsic loss tangent $\tan\delta_i \approx 3\times10^{-3}$. This number is typical of amorphous oxide thin films.

The dielectric loss of TLS can influence the qubit T_1 time in two ways. First, lossy dielectrics incorporated in the wiring external to the qubit junction contribute a fraction α to the qubit capacitance. In the moderately complex phase qubit circuits studied to date, one requires an amorphous dielectric to act as a wiring insulator; in this case, the contribution of the parasitic capacitance of the wiring insulator to the qubit junction self-capacitance can be as large as 10%. However, even in simpler flux and charge qubit circuits fabricated in a single double-angle evaporation step, the lossy native oxides of the superconducting metals make a non-negligible contribution to the effective capacitance of the junction. The dissipation from the amorphous dielectric can be expressed as a lossy capacitance αC in parallel with the junction. In this case, the real part of the effective admittance shunting the junction becomes

$$\mathrm{Re}\;Y(\omega_{10}) = \alpha\,\omega_{10}C\;\tan\delta_i \tag{23}$$

and the qubit energy relaxation time is given by

$$T_1 = 1/(\alpha\,\omega_{10}\tan\delta_i). \tag{24}$$

These expressions make it clear that it will be difficult to engineer a quantum resonator with Q of order 10^6 using materials with intrinsic Q of order 10^3.

Second, in the case of a large qubit junction with area $\gtrsim 100\;\mu$m^2, the tunnel barrier itself contains a quasicontinuum of resonant TLS, and dissipation from these states can induce qubit energy relaxation. In this case, the qubit T_1 is given by (24) with $\alpha = 1$, and where $\tan\delta_i$ now refers to the lossy tunnel barrier dielectric. The large intrinsic loss tangent of amorphous AlO_x accounts for the relatively short coherence times $\sim$10 ns of the first-generation large-area phase qubit circuits [6].

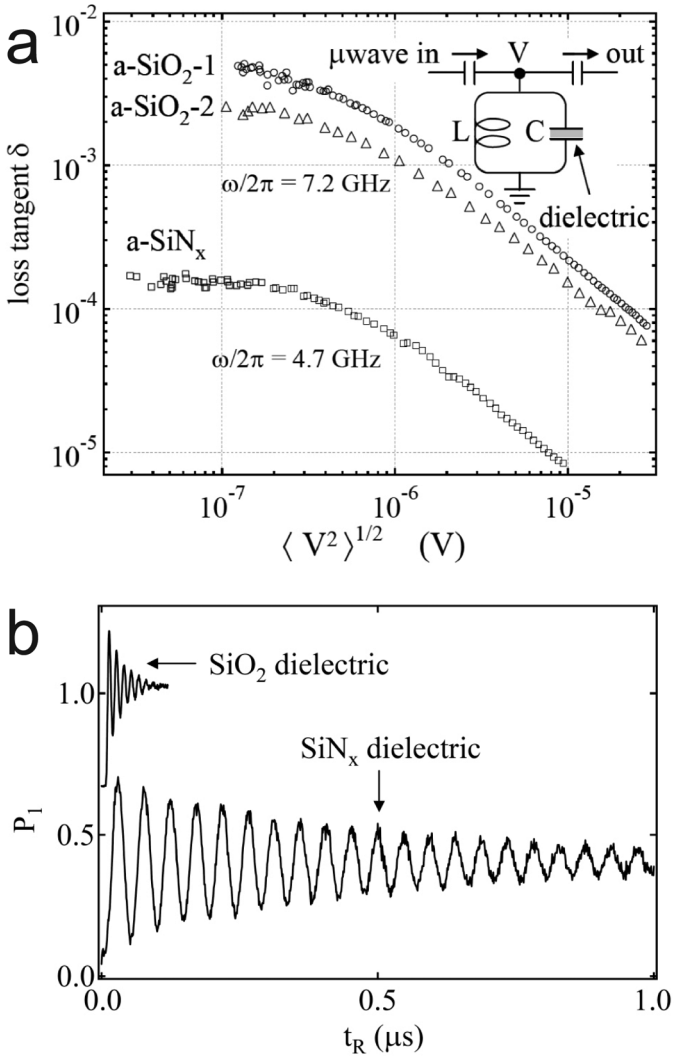

Fig. 3. Microwave loss induced by TLS. (a) Dielectric loss tangents of PECVD-deposited SiO_2 and SiN_x measured at millikelvin temperature as a function of microwave drive power. Measurement circuit is shown in inset. (b) Rabi oscillations for phase qubit circuits incorporating PECVD-grown SiO_2 and SiN_x wiring dielectrics. The factor 20 improvement in loss tangent for the SiN_x compared to the SiO_2 yields a factor 20 enhancement in qubit energy relaxation time. Reprinted figures with permission from [29]. Copyright 2005 by the American Physical Society.

It is straightforward to probe the intrinsic loss of candidate dielectric materials by fabricating and characterizing thin-film linear LC tank circuits in which the material under study forms the capacitor dielectric. At millikelvin temperatures and at low microwave drive powers, the internal quality factor of the tank is the inverse of the intrinsic loss tangent of the capacitor dielectric: $Q_i = 1/\tan\delta_i$. Such measurements were used to demonstrate the high intrinsic loss of the plasma-enhanced chemical vapor deposition (PECVD)-grown SiO_2 films used in first-generation phase qubit circuits [29]. While at present there is no detailed understanding of the microscopic materials origin of dielectric TLS, it is clear that a high density of OH defects in amorphous dielectrics leads to significant dissipation at microwave frequencies. Previous experiments on bulk samples of doped quartz revealed a dielectric loss tangent that scaled linearly with OH impurity concentration [25]. Typical PECVD-grown SiO_2 films are expected to contain OH impurities of a few atomic percent [33], and the measured loss tangents in these thin films are compatible with an extrapolation of the bulk measurements on doped quartz. By contrast, PECVD-grown SiN_x films grown from SiH_4 and N_2 precursors display intrinsic dielectric loss tangents more than a factor of 20 lower than SiO_2 films grown in the same deposition system [Fig. 3(a)]. Substitution of low-loss SiN_x for lossy SiO_2 in an otherwise identical phase qubit circuit leads to an enhancement in qubit energy relaxation time by a factor of 20 [Fig. 3(b)] [29].

A recent survey of several candidate dielectrics for qubit circuits indicates that, among amorphous dielectrics, amorphous silicon hydride (a-Si:H) has a particularly low intrinsic loss tangent of order 10^{-5}[34]. This result is compatible with data on acoustic attenuation in a-Si:H and a-Ge:H that suggest a TLS density of states that is two orders or magnitude lower than that of typical glass films [27]. There has been speculation that the fourfold coordination in these covalently bonded films tends to overconstrain atomic-scale defect states and thereby suppress the density of low-energy excitations [35].

Clearly, it is desirable for the capacitance shunting the qubit junction to be entirely free of low-energy defect states. Efforts to incorporate defect-free, crystalline dielectric thin films into qubit circuits are underway, and some recent successes are described in the following section. At the same time, a scalable superconducting qubit architecture, involving a complex circuit topology with numerous wiring interconnects, will most likely require a reliable, low-loss amorphous wiring dielectric. Optimization of the growth of the amorphous dielectric films for this purpose will require a deeper understanding of the microscopic physics that drives TLS-induced microwave loss, and a thorough exploration of the phase space for dielectric film growth.

V. Fidelity Loss From TLS

While a continuum of TLS in bulk dielectrics can lead to energy relaxation, coupling of the qubit to discrete TLS in the Josephson tunnel barrier itself can lead to the quantum coherent transfer of energy between the qubit and the TLS, and result in fidelity loss. The interaction of the TLS dipole moment with the resonant electric field of the junction capacitance is described by the following Hamiltonian:

$$H_{\rm int} = i\frac{S}{2}(|0e\rangle\langle 1g| - |1g\rangle\langle 0e|) \tag{25}$$

where

$$S = 2\frac{d}{ex}\sqrt{\hbar\omega_{10}\frac{e^2}{2C}}\ \cos\eta\ \sin\theta \tag{26}$$

and where x is the thickness of the tunnel barrier dielectric. One expects to find a broad distribution of coupling matrix elements, due to the dependence of the interaction on both the orientation η of the TLS dipole moment and the TLS asymmetry parameter θ.

The coupling of the qubit to discrete TLS can be observed both spectroscopically and in the time domain. Interaction between the qubit and a resonant TLS gives rise to an avoided level crossing in the qubit spectroscopy [36]; the size of the energy splitting is simply S/h. Spectroscopy of the qubit performed over a broad range of frequencies reveals a density of TLS-induced splittings around 0.5 $\mathrm{GHz}^{-1}\,\mu\mathrm{m}^{-2}$; these splittings have been observed in phase qubits, flux qubits, and charge qubits. In the case of phase qubits with large junction area of

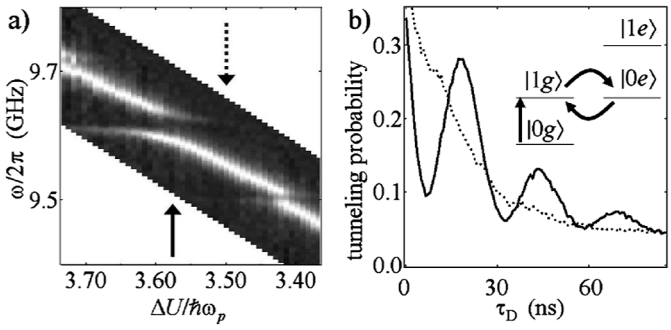

Fig. 4. (a) Phase qubit spectroscopy showing TLS-induced avoided level crossings with size $S/h = 44$ MHz and 24 MHz. (b) Coherent quantum oscillations between a phase qubit and a single resonant TLS in the tunnel barrier. Solid (dashed) trace was acquired at the bias point indicated by the solid (dashed) arrow in part (a), corresponding to resonant (nonresonant) bias. Reprinted figure with permission from [37]. Copyright 2004 by the American Physical Society.

order 100 μm^2, qubit T_1 is directly determined by the loss tangent of the tunnel barrier dielectric: $T_1 = 1/(\omega_{10} \tan\delta_i)$. For smaller-area charge or flux qubits, the density of splittings is reduced, due to the reduced junction area. However, due to the $1/\sqrt{C}$ scaling of the coupling matrix element (26), the coupling of the qubit to any TLS that might be present is likely to be large, and in some cases may preclude normal operation of the qubit. It is probable that the reduced yield of charge and flux qubits as compared to phase qubits is due to the occasional presence of dominant TLS fluctuators in the junction barrier.

To observe the coherent interaction between the qubit and the TLS in the time domain, one can promote the qubit from the $|0\rangle$ state to the $|1\rangle$ state. Because the state $|1g\rangle$ is not an eigenstate of the interaction Hamiltonian (25), the state undergoes free precession in the subspace spanned by $|1g\rangle$ and $|0e\rangle$; as a result, there is a coherent beating in the probability of occupation of the $|1\rangle$ state, instead of the exponential decay typically encountered in the case of an inversion recovery sequence (Fig. 4) [37]. Recent work has demonstrated the use of a single TLS as a quantum memory, and the fidelity of the memory operation has been evaluated tomographically [38].

While the spurious coupling of the qubit to resonant TLS can be suppressed by operating the qubit so that it is far detuned from dominant TLS defect states, in many instances it is necessary to tune the qubit frequency, either to perform measurement or to realize fast gate operations. In this case, the qubit resonance is swept through the resonance frequencies of adjacent TLS. For a finite bias sweep rate, there is the possibility that the state adiabatically evolves from $|1g\rangle$ to $|0e\rangle$: the excitation is then swapped from the qubit to the TLS, with associated loss in the fidelity of the qubit operation. For a bias sweep rate $d\omega_{10}/dt$ through an energy anticrossing of size S, the probability of a (fidelity-preserving) Landau–Zener transition is given by

$$P_{|1g\rangle \to |1g\rangle} = \exp\left[-\pi S_i^2 / 2\hbar^2 \left(d\omega_{10}/dt\right)\right]. \qquad (27)$$

In the limit as the number of resonances becomes very large, it is possible to show that

$$P_{|1g\rangle \to |1g\rangle} \approx \exp(-\omega_{10} t_p \tan\delta_i) \qquad (28)$$

where $\tan\delta_i$ is the intrinsic loss tangent of the tunnel barrier dielectric, and where t_p is the duration of the bias pulse. For example, in the case of a large-area phase qubit circuit with $\omega_{10}/2\pi = 10$ GHz and with $\tan\delta_i = 2 \times 10^{-3}$ for the tunnel barrier, equation (27) predicts a 50% measurement fidelity for a 5-ns measurement pulse. This estimate is compatible with the measurement fidelities obtained in first-generation phase qubits.

While TLS-induced fidelity loss has been most thoroughly investigated in the context of the large-area phase qubit, it has also been studied in the quantronium qubit [39]. In this case, radio-frequency irradiation during readout with the Josephson bifurcation amplifier induces a Stark shift that carries the qubit resonance through neighboring TLS states, causing qubit depolarization by the mechanism described above.

In order to minimize fidelity loss due to TLS in the qubit tunnel barrier, it is necessary to reduce the density of resonant TLS. This can be achieved in a straightforward way by reducing the area of the Josephson junction. However, reduction in junction area leads to an increase in the coupling matrix element between the qubit and the TLS, as can be seen from equation (25). This problem can be circumvented by reducing the area of the junction, and then shunting the junction with a thin-film capacitor to maintain the same coupling matrix element between the junction and any remaining TLS. This strategy was employed successfully in the second-generation phase qubit circuits described in [41]. The resulting devices displayed measurement fidelity approaching 90%, sufficient to perform high-fidelity tomography on a coupled phase qubit circuit [42].

An alternative approach is to reduce the density of TLS by improving the quality of the barrier material. Nearly all superconducting qubits studied to date have employed an amorphous aluminum oxide barrier. Studies of $1/f$ junction critical-current noise suggest that the TLS densities in all amorphous oxide barriers are similar [23] (see below). Therefore, reduction of the defect density in the junction will likely require a radically new approach to junction fabrication. One approach is to employ a defect-free, single crystalline barrier for the Josephson junction. While the epitaxial growth of an insulator on a metal is a daunting challenge, there has been some progress in the molecular beam epitaxy growth of Re–Al_2O_3–Al junctions with epitaxial barriers [43], [44]. Re and Al_2O_3 are lattice-matched to within 1%; however, growth conditions must be optimized to prevent formation of three-dimensional clusters and promote the two-dimensional growth of the oxide. The critical step is to evaporate the Al at low temperature in a small partial pressure of 1×10^{-6} Torr of O_2, and then to crystallize the oxide with a high temperature anneal at 800 °C in 4×10^{-6} Torr of O_2 (Fig. 5). The epitaxial Re–Al_2O_3–Al junctions display a density of TLS reduced by a factor of five with respect to a typical amorphous junction [40]. There is a suspicion that the remaining TLS reside at the amorphous oxide formed at the interface of the crystalline Al_2O_3 and the amorphous Al counterelectrode, which is grown at low temperature. It is possible that more advanced growth techniques could circumvent this problem.

VI. Dephasing From Critical-Current Noise

The Josephson energy $E_J \equiv I_0\Phi_0/2\pi$ is a critical parameter determining the qubit energy landscape; for this reason, all superconducting qubits are susceptible to dephasing from excess low-frequency critical-current noise. $1/f$ critical-current fluctuations have been studied for decades in the context of efforts to realize low-noise SQUIDs [45]–[47]. The noise is widely believed to arise from charged TLS in the tunnel barrier that locally modify the barrier transmissivity [48] (Fig. 6). A recent

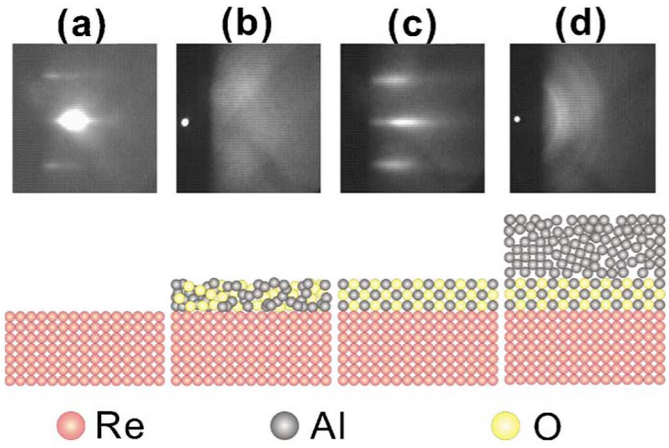

Fig. 5. Reciprocal images and real-space figures of the growth sequence for epi-Re/epi-Al_2O_3/polycrystal-Al barriers. (a) Epitaxial Re grown at 850 °C on a sapphire (0001) substrate. The streaks in the RHEED image indicate that the film is single crystalline. (b) Amorphous AlO_x tunnel barrier reactively evaporated onto the base Re film at room temperature. (c) Epitaxial Al_2O_3 formed after an 800 °C anneal of the amorphous AlO_x. (d) Polycrystalline Al counterelectrode. Reprinted figure with permission from [40]. Copyright 2006 by the American Physical Society.

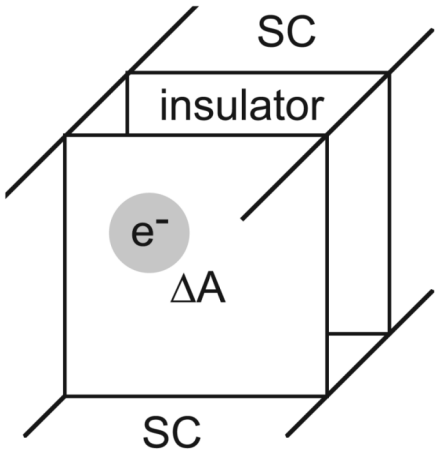

Fig. 6. Schematic of Josephson tunnel barrier, indicating fluctuating charged defect that modulates the junction effective area by ΔA.

survey analyzed data on Josephson tunnel barriers of different areas, transmissivities, and fabricated in different amorphous technologies [23]. Based on the assumption of independent TLS fluctuators, it was expected that the noise from junctions fabricated in the same technology should scale as $S_{I_0} \propto I_0^2/A$, where A is the junction area; this scaling was indeed observed. More surprisingly, it was found that all amorphous tunnel barriers show roughly the same levels of critical-current noise at 4.2 K

$$A^{1/2} S_{I_0}^{1/2}(1\ \mathrm{Hz})/I_0 \approx 10\ \mu\mathrm{m\ pA/Hz^{1/2}}/\mu\mathrm{A}. \qquad (29)$$

This suggests some underlying universality of the TLS density and of the microscopic physics that drives TLS fluctuations. At present, however, the microscopic origin of the junction noise is not completely understood.

Of particular interest in this connection are experiments that probe the temperature dependence of the $1/f$ critical-current noise. Wellstood *et al.* characterized the critical-current noise of resistively shunted Josephson junctions from 90 mK to 4.2 K, and found that the noise scaled with temperature as T^2[49]. On the other hand, a recent investigation of the resistance fluctuations of normal conducting Al–AlO_x–Al tunnel junctions [50] revealed a linear in T dependence of the junction noise, with a magnitude at 4 K that was two orders of magnitude lower than the noise expected from (29), assuming that the critical-current noise is due to underlying fluctuations of the tunnel resistance. The recent model of [51] explains this discrepancy in terms of a new noise mechanism that plays a role only in the superconducting state, and which adds to the conventional noise produced by TLS in the tunnel barrier. Namely, it is supposed that there are localized subgap states that form below T_c at the superconductor-insulator boundary, and between which electrons can tunnel. The T^2 dependence of the noise and the observed noise magnitude are both compatible with this model.

As a final note, we remark that measurements on the critical-current noise of an rf SQUID operated in the dispersive mode (so that the junction is maintained in the supercurrent state) reveal a junction noise magnitude similar to that observed in experiments where the junction is biased in the finite voltage state [52]. Thus, it is expected that critical-current noise will ultimately limit the dephasing times of superconducting qubits. For example, assuming a T^2 dependence of the critical-current noise and taking the 4.2 K noise magnitude of (29), one expects to find a dephasing time of order 10 μs for typical phase qubit circuits [10]. At present, however, none of the superconducting qubit implementations is limited by critical-current noise. Depending on the specific qubit type, transverse relaxation times are limited by dephasing due to excess low-frequency charge noise or flux noise (see below), or by dissipation.

It is expected that the development of crystalline, defect-free tunnel barriers will lead to Josephson junctions with a greatly reduced level of $1/f$ noise. Despite recent progress in the development of crystalline barriers [43], [44], to our knowledge there have been no experiments to investigate $1/f$ noise in these junctions.

VII. Dephasing From Charge Noise

In the case of small-area Josephson charge qubits, low-frequency fluctuations of the background charge can be a major source of qubit dephasing. The charge qubit Hamiltonian takes the form $H = (-\Delta E/2)[\sigma_z \cos\theta + \sigma_x \sin\theta]$, where $\theta \equiv -\arctan(E_J/\Delta U)$ and $\Delta E \equiv \sqrt{\Delta U^2 + E_J^2}$ are determined by the electrostatic energy difference ΔU between the charge states and by the Josephson energy E_J. Charge noise creates spurious fluctuations of the electrostatic bias ΔU, resulting in uncontrolled accumulation of phase between the qubit states. Low-frequency charge noise has been studied extensively in single-electron transistors (SETs); it is seen that the power spectral density of charge noise scales with frequency as $1/f$, with a magnitude at 1 Hz of order $(10^{-3}e)^2/\mathrm{Hz}$ [30]. The charge noise observed in SETs is compatible with the measured coherence times of order 100 ps observed in the first charge qubit free-induction decay experiments [53]. These experiments further demonstrated that echo sequences can substantially suppress inhomogeneous dephasing due to low-frequency charge noise.

Low-frequency charge noise is typically understood to arise from the trapping and detrapping of single electron charges in the amorphous insulators in the vicinity of the qubit. From

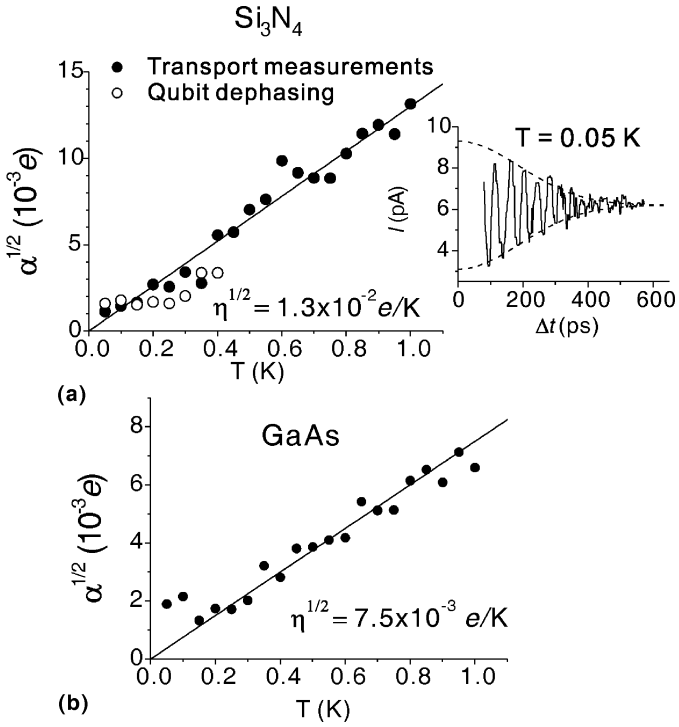

Fig. 7. (a) $1/f$ charge noise magnitude $\alpha^{1/2}$ versus temperature, obtained from SET transport (solid symbols) and from qubit dephasing (open symbols; see inset). The device was fabricated on CVD-grown Si_3N_4. (b) As in (a), for an SET fabricated on a GaAs substrate. Reprinted figure with permission from [56]. Copyright 2006 by the American Physical Society.

Green's reciprocity theorem, the change in gate voltage induced by a fluctuating charge at position $\vec{x}$ is proportional to the electric field induced at $\vec{x}$ by a charge on the qubit island. Researchers observe TLS that induce offset charges that are a substantial fraction of an electron charge; the authors of [54] take this as evidence that the dominant TLS are located in the barrier of the Josephson junction, where the electric fields are the highest. On the other hand, there is evidence based on noise correlation measurements performed on a pair of SETs operated in close proximity that a substantial fraction of the noise comes from fluctuating charged TLS in the amorphous dielectrics or substrate surrounding the SETs [55]. The temperature dependence of the excess low-frequency charge noise has recently been characterized over a temperature range from 200 mK to 1 K, and a T^2 scaling of the noise was observed [56] (Fig. 7). A T^2 scaling was predicted by the authors of [57] based on a model of thermal activation of TLS from asymmetric double-well potentials. An alternative explanation is based on an assumed linear dependence $D(\omega) \propto \omega$ of the defect density of states on frequency [58]. While this form of the density of states is a departure from the standard TLS model [see (12)], it arises naturally in models of localized states coupled to a metallic reservoir [59]. The authors of [58] further outline a deep connection between low-frequency fluctuations and high-frequency dissipation induced by TLS in the thermal and quantum regimes, respectively. This connection yields a crossover from a $1/f$ noise spectrum to an ohmic ($\propto f$) spectrum at a frequency $\omega_c \approx k_B T/\hbar$; such a crossover is compatible with detailed experiments on the relaxation and dephasing of charge qubits [60].

Despite this recent progress in the phenomenological description of the charge noise, a detailed microscopic picture is still lacking. And while there is some indication that charge noise is lower in SETs that are electrostatically isolated from the substrate [61], there has been little progress in the the development of novel materials or circuit designs that display a reduced level of charge noise. However, robust techniques have been developed to suppress qubit sensitivity to charge fluctuations. The sensitivity of the qubit to charge noise is determined by the transfer function $\partial\omega_{10}/\partial n_g$, where $n_g \equiv C_g U/2e$ is the reduced gate charge of the island. At a charge bias $n_g = 1/2$, it is equally favorable energetically for zero or one excess Cooper pair to reside on the island, and $\partial\omega_{10}/\partial n_g$ vanishes: at this optimal working point, the qubit is insensitive to charge noise to first order. The "quantronium" qubit of the Saclay group was the first to successfully exploit an optimal working point strategy to decouple to the qubit from low-frequency bias fluctuations [62]; in fact, this qubit possessed a "sweet spot" in both the gate charge and the phase directions, rendering the qubit relatively insensitive to $1/f$ fluctuations of both background charge and flux. The quantronium qubit achieved long T_2^* times of order 1 μs at the optimal working point. Moreover, systematic investigations of quantronium dephasing away from the optimal working point have been used as a sensitive probe of low-frequency bias noise [17]. In particular, it is seen that dephasing away from optimal charge bias can be explained by a $1/f$ charge noise of order $(10^{-3}e)^2/\text{Hz}$ at 1 Hz, provided one invokes a sharp cutoff of the charge noise power spectral density at around 0.4 MHz. In the Bloch–Redfield picture of decoherence [16], this ultraviolet cutoff is related to a lower cutoff of the relaxation time distribution of the underlying thermal TLS [58].

In a further refinement, researchers at Yale implemented a capacitively shunted split Cooper pair box qubit coupled to a transmission line resonator, the so-called "transmon" qubit [63], [64]. The addition of the capacitive shunt reduces the qubit charging energy, thereby reducing the curvature of the qubit energy bands and decreasing sensitivity to charge noise. A key to this design is the fact that sensitivity to charge noise decreases exponentially as E_J/E_C is increased, while the anharmonicity of the qubit levels decreases as a weak power law [63]. With this scheme a "sweet spot" is realized at all values of gate charge, and inhomogeneous broadening is drastically suppressed. Transverse relaxation in the transmon appears to be limited by dissipation, due presumably to dielectric losses in the amorphous surface oxides of the circuit [65].

VIII. Dephasing From Flux Noise

In the Josephson flux and phase qubits, low-frequency excess flux noise is a dominant source of qubit dephasing. In the Josephson flux qubit, the Gaussian decay envelope of qubit Ramsey fringes is compatible with a magnetic flux noise with $1/f$ spectrum and a magnitude at 1 Hz of 1 $\mu\Phi_0/\text{Hz}^{1/2}$[66], [67] (Fig. 8). In the Josephson phase qubit, a recent experiment used the resonant response of the qubit to measure the power spectral density of magnetic flux noise directly; again the spectrum was $1/f$, with a noise magnitude comparable to that seen in the flux qubit [68]. While these experiments identify flux noise as a dominant dephasing mechanism, they offer no clue to its microscopic origin.

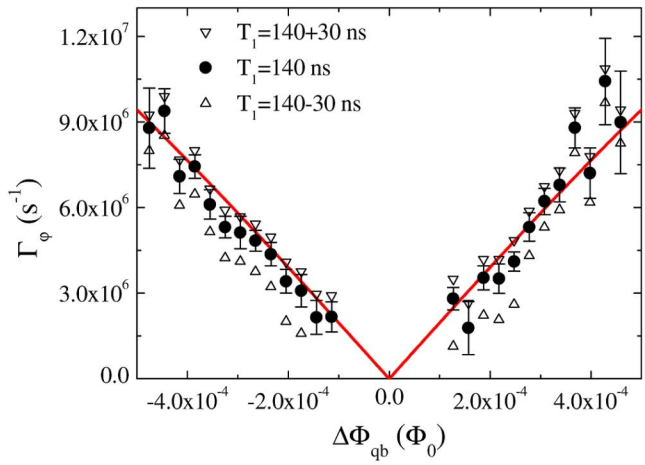

Fig. 8. Dephasing in a flux qubit. The linear dependence of dephasing rate Γ_ϕ on flux offset $\Delta\Phi_{qb}$ from the degeneracy point suggests a low-frequency $1/f$ flux noise with magnitude of order $10^{-12}\ \Phi_0^2/\mathrm{Hz}$ at 1 Hz. The dephasing rates are extracted from a fit to the Gaussian decay envelope of qubit echo signals, assuming the T_1 values shown. Reprinted figure with permission from [67]. Copyright 2007 by the American Physical Society.

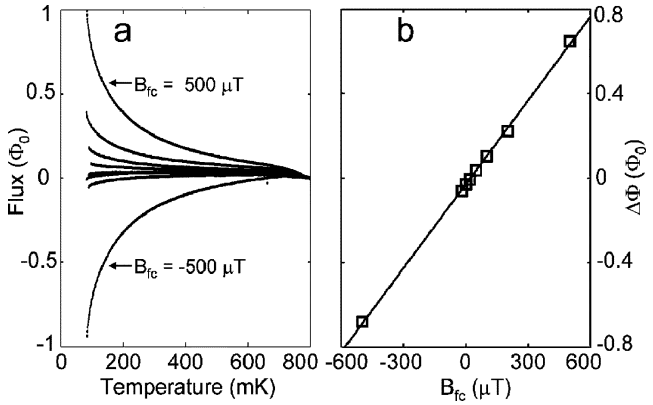

Fig. 9. Surface magnetism in a dc SQUID. (a) Temperature-dependence of flux threading a Nb SQUID, for different fields B_{fc} applied as the device was cooled through T_c (from bottom to top, $B_{fc} = -500, -20, 0, 20, 50, 100, 200, 500\ \mu$T). (b) Temperature-induced flux change $\Delta\Phi = \Phi(100\ \mathrm{mK}) - \Phi(500\ \mathrm{mK})$ on cooling from 500 to 100 mK versus cooling field B_{fc}. The data indicates a surface density of unpaired electron spins of $5 \times 10^{17}\ \mathrm{m}^{-2}$. Reprinted figure with permission from [70]. Copyright 2008 by the American Physical Society.

The flux noise inferred from recent qubit experiments is consistent with the flux noise observed more than 20 years ago in a series of measurements performed on dc SQUIDs cooled to millikelvin temperatures [69]. The noise was observed to be "universal," that is, only weakly dependent on a wide range of parameters such as superconducting materials, overall scale of the SQUID loop, and temperature. While these experiments ruled out many potential sources of noise, the microscopic mechanism was never identified.

Recent experiments have revealed clear evidence for a high density of unpaired surface spins in thin-film SQUIDs [70], and suggest that these spins are the source of the excess low-frequency flux noise. While fluctuations of the spins give rise to noise at the 1 $\mu\Phi_0$ level, the coherent magnetization of the spins couples a surprisingly large flux of order 1 Φ_0 to the SQUID. In these experiments, a Nb SQUID was cooled through T_c in an applied magnetic field in order to intentionally trap vortices in the film. The SQUID was subsequently operated in a flux-locked loop and cooled to millikelvin temperatures. The flux threading the SQUID increased as $1/T$ as temperature was lowered (Fig. 9); moreover, the flux change was proportional to the density of trapped vortices. The data is compatible with the thermal polarization of unpaired surface spins in the trapped fields of the vortices. From the magnitude of the temperature-dependent flux change, a surface spin density of $5 \times 10^{17}\ \mathrm{m}^{-2}$ was inferred. This density of surface spins is compatible with the surface spin density postulated in a recent model for spin-flip scattering that has been proposed [71] to account for the magnetic-field enhancement of the critical-current of superconducting nanowires [72]. Moreover, this spin density is compatible with densities inferred from electron spin resonance studies of the disordered Si-SiO_2 interface [73]. Thus, it is not unreasonable that spin densities of this order exist at the interface between the insulating substrate and the superconductor, or between the superconductor and its insulating native oxide.

There has been considerable recent theoretical interest in the possibility that the $1/f$ flux noise is due to surface spins [63], [73], [74]. Models for $1/f$ flux noise from surface spins are attractive, as they yield a noise power that is only weakly dependent on the overall scale of the device, compatible with the "universal" character of the noise [68]. In fact, as we show now, an extremely simplistic calculation of the noise from surface spins yields the correct magnitude and scaling, starting only from the assumption of a log-uniform distribution of spin relaxation times. We begin by considering an ensemble of spins with relaxation time τ. The spin susceptibility $\chi_\tau(\omega) = \chi'_\tau(\omega) - i\chi''_\tau(\omega)$ takes on the familiar Lorentzian form

$$\chi'_\tau(\omega) = \frac{n\mu_0\mu_B^2}{2k_BT}\ \frac{1}{1+\omega^2\tau^2}$$
$$\chi''_\tau(\omega) = \frac{n\mu_0\mu_B^2}{2k_BT}\ \frac{\omega\tau}{1+\omega^2\tau^2} \tag{30}$$

where n is the spin density, and where the subscripts τ indicate that we are referring to spins with a single relaxation time τ. The imaginary part of the spin susceptibility, a direct consequence of the nonzero spin relaxation time, leads to hysteresis in the spin magnetization for a finite excitation frequency, and thus represents dissipation.

In many spin systems, we expect to find a log-uniform distribution of spin relaxation times [75]. That is, we have a relaxation time distribution given by

$$g(\tau) = \frac{1}{\ln(\tau_2/\tau_1)}\ \frac{1}{\tau} \tag{31}$$

where τ_1 and τ_2 are lower and upper cutoffs for the spin relaxation times, respectively. In this case, the frequency-dependent spin susceptibility is given by

$$\chi(\omega) = \chi_0 \int_{\tau_1}^{\tau_2} g(\tau)\ \frac{1}{1+i\omega\tau}\, d\tau \tag{32}$$

where $\chi_0 \equiv n\mu_0\mu_B^2/2k_BT$. Performing the integration in the limit $1/\tau_2 \ll \omega \ll 1/\tau_1$, we find

$$\chi(\omega) \approx \frac{\chi_0}{\ln(\tau_2/\tau_1)}\left[-\ln(\omega\tau_1) - i\frac{\pi}{2}\right]. \tag{33}$$

We see that the dissipative part of the spin susceptibility is frequency-independent and given by

$$\chi'' = \frac{\pi}{2}\frac{\chi_0}{\ln(\tau_2/\tau_1)}. \tag{34}$$

Now we relate the imaginary part of the spin susceptibility of surface spins to $1/f$ flux noise in a SQUID. We consider a simple toroidal model of a SQUID with loop radius R and wire radius r, covered with a surface density of spins σ. We use reciprocity to calculate the coupling of the surface spins to the SQUID, and this enables us to calculate the spin contribution to the SQUID inductance. The spin contribution to the inductance has both real and imaginary parts; the imaginary part of the SQUID inductance is given by

$$L_s'' = \frac{\pi}{2}\frac{1}{\ln(\tau_2/\tau_1)} L_0 \tag{35}$$

where

$$L_0 = \frac{\mu_0^2\mu_B^2}{2k_BT}\,\sigma\,\frac{R}{r}. \tag{36}$$

From the fluctuation-dissipation theorem, we can directly relate this frequency-independent imaginary inductance to $1/f$ noise

$$\begin{aligned} S_\Phi(f) &= \frac{2k_BTL_s''}{\pi f} \\ &= \frac{1}{2\ln(\tau_2/\tau_1)}\,\mu_0^2\mu_B^2\,\sigma\,\frac{R}{r}\,\frac{1}{f}. \end{aligned} \tag{37}$$

For example, for $R/r = 10$, $\tau_2/\tau_1 = 10^{10}$, and $\sigma = 5 \times 10^{17}$ m^{-2} [4], we find $L_s'' = 16$ aH at $T = 100$ mK, and $S_\Phi^{1/2}(1\text{ Hz}) = 2\ \mu\Phi_0/\text{Hz}^{1/2}$ [4], independent of temperature.

Thus, from a very simple set of assumptions, one reproduces the magnitude and key features of the observed flux noise: the noise is independent on the overall scale of the device, and roughly independent of temperature. The first feature is a consequence of the fact that the fluctuating spins reside on the surface, while the latter fact results from the $1/T$ paramagnetic prefactor in the spin susceptibility.

While the above picture perhaps captures some of the basic physics of the excess flux noise, it is clearly an oversimplification. For example, this description neglects the possibility of interactions between surface spins, despite the fact that experimental evidence indicates that interactions between spins are significant [70]. A recent flux noise model considers spins at the superconductor-insulator interface that interact via the RKKY mechanism, and which diffuse in the nonuniform surface magnetic fields of the SQUID [74]; in this case, interactions between spins are essential to the noise mechanism.

At present there is no clear understanding of the precise microscopic nature of the surface spin states that give rise to the excess flux noise, although this is an active area of current research. It is possible that novel surface treatments of the superconducting thin films could be used to suppress the surface spin density. Alternatively, the application of a strong local magnetic field could polarize the surface spins and thereby suppress spin fluctuations. In the absence of improved, low-defect surfaces, optimal working point strategies have been employed to realize flux qubits with long transverse relaxation times of order 1 μs [14].

IX. Conclusion

Less than ten years have passed since the first observation of coherent quantum oscillations in superconducting charge, flux, and phase qubits; however, the progress over this interval has been considerable. There have been demonstrations of transverse relaxation times in excess of 1 μs [14], [62], [65], the realization of adjustable coupling of qubits [76], [77], the demonstration of state tomography of coupled qubits [42], and investigations of the coherent interaction of superconducting qubits with cavity photon states [20], [78], [79]. Moreover, there has been significant progress in understanding the underlying physics that governs qubit dissipation and decoherence, and already this increased understanding has been leveraged to develop novel materials and novel circuit designs with improved coherence times. For qubit circuits that are adequately decoupled from the dissipation of the leads, TLS-induced loss in the amorphous dielectrics of the circuit remains a dominant relaxation channel. Continued optimization of the amorphous qubit dielectrics and the reliable incorporation of crystalline dielectrics into qubit circuits are required to support sustained improvements in qubit relaxation times and fidelity. At the same time, the microscopic mechanisms that govern critical-current, charge, and flux noise are not fully understood, and further experimental and theoretical investigations are required to provide direction in the search for improved low-noise materials and circuit designs.

As a final note, it is useful to recall that the explosion of the semiconductor industry over the second half of the 20th Century was fueled by the exhaustive materials research that enabled the robust growth of high-quality silicon single crystals and optimization of the Si-SiO_2 interface. The superconducting qubit community now demands a similar focus on the development of high-quality, low-noise materials. Many of the key materials issues that limit qubit performance have now been identified, and researchers have only begun to explore the available phase space for the growth of optimized materials. It is reasonable to think that the continued development of qubit materials will yield significant improvements in qubit coherence and fidelity, and thereby facilitate realization of scalable quantum information processing with superconducting circuits.

Acknowledgment

The author thanks J. M. Martinis and B. L. T. Plourde for helpful discussions.

References

[1] M. A. Nielsen and I. L. Chuang, *Quantum Computation and Quantum Information*. Cambridge, U.K.: Cambridge Univ. Press, 2000.
[2] M. H. Devoret and J. M. Martinis, "Implementing qubits with superconducting integrated circuits," *Quant. Info. Proc.*, vol. 3, pp. 163–203, 2004.
[3] J. Q. You and F. Nori, "Superconducting qubits and quantum information," *Phys. Today*, vol. 58, p. 42, 2005.
[4] R. J. Schoelkopf and S. M. Girvin, "Wiring up quantum systems," *Nature*, vol. 451, pp. 664–669, 2008.
[5] B. D. Josephson, "Possible new effects in superconductive tunnelling," *Phys. Lett.*, vol. 1, pp. 251–253, 1962.
[6] J. M. Martinis, S. Nam, J. Aumentado, and C. Urbina, "Rabi oscillations in a large Josephson junction qubit," *Phys. Rev. Lett.*, vol. 89, p. 117907, 2002.

[7] A. J. Berkley, H. Xu, R. C. Ramos, M. A. Gubrud, F. W. Strauch, P. R. Johnson, J. R. Anderson, A. J. Dragt, C. J. Lobb, and F. C. Wellstood, "Entangled macroscopic quantum states in two superconducting qubits," *Science*, vol. 300, pp. 1548–1550, 2003.

[8] M. Tinkham, *Introduction to Superconductivity*. New York: McGraw-Hill, 1996.

[9] J. Clarke, A. N. Cleland, M. H. Devoret, D. Esteve, and J. M. Martinis, *Science*, vol. 239, p. 992, 1988.

[10] J. M. Martinis, S. Nam, J. Aumentado, K. M. Lang, and C. Urbina, "Decoherence of a superconducting qubit due to bias noise," *Phys. Rev. B*, vol. 67, p. 094510, 2003.

[11] J. R. Friedman, V. Patel, W. Chen, S. K. Tolpygo, and J. E. Lukens, "Quantum superposition of distinct macroscopic states," *Nature*, vol. 406, pp. 43–46, 2000.

[12] C. H. van der Wal, A. C. J. ter Haar, F. K. Wilhelm, R. N. Schouten, C. J. P. M. Harmans, T. P. Orlando, S. Lloyd, and J. E. Mooij, "Quantum superposition of macroscopic persistent-current states," *Science*, vol. 290, pp. 773–777, 2000.

[13] V. Bouchiat, D. Vion, P. Joyez, D. Esteve, and M. H. Devoret, "Quantum coherence with a single Cooper pair," *Phys. Scripta*, vol. T76, p. 165, 1998.

[14] I. Chiorescu, Y. Nakamura, C. J. P. M. Harmans, and J. E. Mooij, "Coherent quantum dynamics of a superconducting flux qubit," *Science*, vol. 299, pp. 1869–1871, 2003.

[15] Y. Nakamura, Y. A. Pashkin, and J. S. Tsai, "Coherent control of macroscopic quantum states in a single-Cooper-pair box," *Nature*, vol. 398, pp. 786–788, 1999.

[16] C. P. Slichter, *Principles of Magnetic Resonance*. Berlin: Springer, 1996.

[17] G. Ithier, E. Collin, P. Joyez, P. J. Meeson, D. Vion, D. Esteve, F. Chiarello, A. Shnirman, Y. Makhlin, J. Schriefl, and G. Schön, "Decoherence in a superconducting quantum bit circuit," *Phys. Rev. B*, vol. 72, p. 134519, 2005.

[18] J. Q. You and F. Nori, "Quantum information processing with superconducting qubits in a microwave field," *Phys. Rev. B*, vol. 68, p. 064509, 2003.

[19] A. Blais, R. S. Huang, A. Wallraff, S. M. Girvin, and R. J. Schoelkopf, "Cavity quantum electrodynamics for superconducting electrical circuits: An architecture for quantum computation," *Phys. Rev. A*, vol. 69, p. 062320, 2004.

[20] A. Wallraff, D. I. Schuster, A. Blais, L. Frunzio, R. S. Huang, J. Majer, S. Kumar, S. M. Girvin, and R. J. Schoelkopf, "Strong coupling of a single photon to a superconducting qubit using circuit quantum electrodynamics," *Nature*, vol. 431, pp. 162–167, 2004.

[21] P. Dutta and P. M. Horn, "Low-frequency fluctuations in solids $1/f$ noise," *Rev. Mod. Phys.*, vol. 53, pp. 497–516, 1981.

[22] C. T. Rogers and R. A. Buhrman, "Composition of $1/f$ noise in metal-insulator-metal tunnel junctions," *Phys. Rev. Lett.*, vol. 53, pp. 1272–1275, 1984.

[23] D. J. Van Harlingen, T. L. Robertson, B. L. T. Plourde, P. A. Reichardt, T. A. Crane, and J. Clarke, "Decoherence in Josephson-junction qubits due to critical-current fluctuations," *Phys. Rev. B*, vol. 70, p. 064517, 2004.

[24] R. C. Zeller and R. O. Pohl, "Thermal conductivity and specific heat of noncrystalline solids," *Phys. Rev. B*, vol. 4, pp. 2029–2041, 1971.

[25] M. von Schickfus and S. Hunklinger, "Dielectric coupling of low-energy excitations in vitreous silica to electromagnetic waves," *J. Phys. C*, vol. 9, pp. L429–L442, 1976.

[26] , W. A. Phillips, Ed., *Amorphous Solids: Low-Temperature Properties*. New York: Springer, 1981.

[27] R. O. Pohl, X. Liu, and E.-J. Thompson, "Low-temperature thermal conductivity and acoustic attenuation in amorphous solids," *Rev. Mod. Phys.*, vol. 74, p. 991, 2002.

[28] M. B. Weissman, "$1/f$ noise and other slow, nonexponential kinetics in condensed matter," *Rev. Mod. Phys.*, vol. 60, pp. 537–571, 1988.

[29] J. M. Martinis, K. B. Cooper, R. McDermott, M. Steffen, M. Ansmann, K. D. Osborn, K. Cicak, S. Oh, D. P. Pappas, R. W. Simmonds, and C. C. Yu, "Decoherence in Josephson qubits from dielectric loss," *Phys. Rev. Lett.*, vol. 95, p. 210503, 2005.

[30] G. Zimmerli, T. M. Eiles, R. L. Kautz, and J. M. Martinis, "Noise in the Coulomb blockade electrometer," *Appl. Phys. Lett.*, vol. 61, pp. 237–239, 1992.

[31] J. Gao, J. Zmuidzinas, B. A. Mazin, H. G. LeDuc, and P. K. Day, "Noise properties of superconducting coplanar waveguide microwave resonators," *Appl. Phys. Lett.*, vol. 90, p. 102507, 2007.

[32] J. Gao, M. Daal, J. M. Martinis, A. Vayonakis, J. Zmuidzinas, B. Sadoulet, B. A. Mazin, P. K. Day, and H. G. Leduc, "A semiempirical model for two-level system noise in superconducting microresonators," *Appl. Phys. Lett.*, vol. 92, p. 212504, 2008.

[33] V. P. Tolstoy, I. Chernyshova, and V. A. Skryshevsky, *Handbook of Infrared Spectroscopy of Ultrathin Films*. Hoboken, NJ: Wiley-VCH, 2003.

[34] A. D. O'Connell, M. Ansmann, R. C. Bialczak, M. Hofheinz, N. Katz, E. Lucero, C. McKenney, M. Neeley, H. Wang, E. M. Weig, A. N. Cleland, and J. M. Martinis, "Microwave dielectric loss at single photon energies and millikelvin temperatures," *Appl. Phys. Lett.*, vol. 92, p. 112903, 2008.

[35] W. A. Phillips, "Tunneling states in amorphous solids," *J. Low Temp. Phys.*, vol. 7, pp. 351–360.

[36] R. W. Simmonds, K. M. Lang, D. A. Hite, S. Nam, D. P. Pappas, and J. M. Martinis, "Decoherence in Josephson phase qubits from junction resonators," *Phys. Rev. Lett.*, vol. 93, p. 077003, 2004.

[37] K. B. Cooper, M. Steffen, R. McDermott, R. W. Simmonds, S. Oh, D. A. Hite, D. P. Pappas, and J. M. Martinis, "Observation of quantum oscillations between a Josephson phase qubit and a microscopic resonator using fast readout," *Phys. Rev. Lett.*, vol. 93, p. 180401, 2004.

[38] M. Neeley, M. Ansmann, R. C. Bialczak, M. Hofheinz, N. Katz, E. Lucero, A. D. O'Connell, H. Wang, A. N. Cleland, and J. M. Martinis, "Process tomography of quantum memory in a Josephson-phase qubit coupled to a two-level state," *Nat. Phys.*, vol. 4, pp. 523–526, 2008.

[39] I. Siddiqi, R. Vijay, M. Metcalfe, E. Boaknin, L. Frunzio, R. J. Schoelkopf, and M. H. Devoret, "Dispersive measurements of superconducting qubit coherence with a fast latching readout," *Phys. Rev. B*, vol. 73, p. 054510, 2006.

[40] S. Oh, K. Cicak, J. S. Kline, M. A. Sillanpää, K. D. Osborn, J. D. Whittaker, R. W. Simmonds, and D. P. Pappas, "Elimination of two level fluctuators in superconducting quantum bits by an epitaxial tunnel barrier," *Phys. Rev. B*, vol. 74, p. 100502, 2006.

[41] M. Steffen, M. Ansmann, R. McDermott, N. Katz, R. C. Bialczak, E. Lucero, M. Neeley, E. M. Weig, A. N. Cleland, and J. M. Martinis, "State tomography of capacitively shunted phase qubits with high fidelity," *Phys. Rev. Lett.*, vol. 97, p. 050502, 2006.

[42] M. Steffen, M. Ansmann, R. C. Bialczak, N. Katz, E. Lucero, R. McDermott, M. Neeley, E. M. Weig, A. N. Cleland, and J. M. Martinis, "Measurement of the entanglement of two superconducting qubits via state tomography," *Science*, vol. 313, pp. 1423–1425, 2006.

[43] S. Oh, K. Cicak, R. McDermott, K. B. Cooper, K. D. Osborn, R. W. Simmonds, M. Steffen, J. M. Martinis, and D. P. Pappas, "Low-leakage superconducting tunnel junctions with a single-crystal Al_2O_3 barrier," *Supercond. Sci. Technol.*, vol. 18, pp. 1396–1399, 2005.

[44] S. Oh, D. A. Hite, K. Cicak, K. D. Osborn, R. W. Simmonds, R. McDermott, K. B. Cooper, M. Steffen, J. M. Martinis, and D. P. Pappas, "Epitaxial growth of rhenium with sputtering," *Thin Solid Films*, vol. 496, pp. 389–394, 2006.

[45] C. T. Rogers and R. A. Buhrman, "Nature of single-localized-electron states derived from tunneling measurements," *Phys. Rev. Lett.*, vol. 55, pp. 859–862, 1985.

[46] R. T. Wakai and D. J. V. Harlingen, "Low-frequency noise and discrete charge trapping in small-area tunnel junction dc SQUIDs," *Appl. Phys. Lett.*, vol. 49, pp. 593–595, 1986.

[47] B. Savo, F. C. Wellstood, and J. Clarke, "Low-frequency excess noise in Nb–Al_2O_3–Nb Josephson tunnel junctions," *Appl. Phys. Lett.*, vol. 50, pp. 1757–1759, 1987.

[48] M. Constantin and C. C. Yu, "Microscopic model of critical current noise in Josephson junctions," *Phys. Rev. Lett.*, vol. 99, p. 207001, 2007.

[49] F. C. Wellstood, C. Urbina, and J. Clarke, "Flicker $(1/f)$ noise in the critical current of Josephson junctions at 0.09–4.2 K," *Appl. Phys. Lett.*, vol. 85, pp. 5296–5298, 2004.

[50] J. Eroms, L. C. van Schaarenburg, E. F. C. Driessen, J. H. Plantenberg, C. M. Huizinga, R. N. Schouten, A. H. Verbruggen, C. J. P. M. Harmans, and J. E. Mooij, "Low-frequency noise in Josephson junctions for superconducting qubits," *Appl. Phys. Lett.*, vol. 89, p. 122516, 2006.

[51] L. Faoro and L. B. Ioffe, "Microscopic origin of critical current fluctuations in large, small, and ultra-small area Josephson junctions," *Phys. Rev. B*, vol. 75, p. 132505, 2007.

[52] M. Mück, M. Korn, C. G. A. Mugford, J. B. Kycia, and J. Clarke, "Measurements of $1/f$ noise in Josephson junctions at zero voltage: Implications for decoherence in superconducting quantum bits," *Appl. Phys. Lett.*, vol. 86, p. 012510, 2005.

[53] Y. Nakamura, Y. A. Pashkin, T. Yamamoto, and J. S. Tsai, "Charge echo in a Cooper-pair box," *Phys. Rev. Lett.*, vol. 88, p. 047901, 2002.

[54] D. Song, A. Amar, C. J. Lobb, and F. C. Wellstood, "Advantages of superconducting Coulomb-blockade electrometers," *IEEE Trans. Appl. Supercond.*, vol. 5, no. 2, pt. 3, pp. 3085–3089, Jun. 1995.

[55] A. B. Zorin, F.-J. Ahlers, J. Niemeyer, T. Weimann, H. Wolf, V. A. Krupenin, and S. V. Lotkhov, "Background charge noise in metallic single-electron tunneling devices," *Phys. Rev. B*, vol. 53, pp. 13682–13687, 1996.

[56] O. Astafiev, Y. A. Pashkin, Y. Nakamura, T. Yamamoto, and J. S. Tsai, "Temperature square dependence of the low frequency $1/f$ charge noise in the Josephson junction qubits," *Phys. Rev. Lett.*, vol. 96, p. 137001, 2006.

[57] M. Kenyon, C. J. Lobb, and F. C. Wellstood, "Temperature dependence of low-frequency noise in Al-Al_2O_3-Al single-electron transistors," *J. Appl. Phys.*, vol. 88, pp. 6536–6540, 2000.

[58] A. Shnirman, G. Schön, I. Martin, and Y. Makhlin, "Low- and high-frequency noise from coherent two-level systems," *Phys. Rev. Lett.*, vol. 94, p. 127002, 2005.

[59] L. Faoro, J. Bergli, B. L. Altshuler, and Y. M. Galperin, "Models of environment and T_1 relaxation in Josephson charge qubits," *Phys. Rev. Lett.*, vol. 95, p. 046805, 2005.

[60] O. Astafiev, Y. A. Pashkin, Y. Nakamura, T. Yamamoto, and J. S. Tsai, "Quantum noise in the Josephson charge qubit," *Phys. Rev. Lett.*, vol. 93, p. 267007, 2004.

[61] V. A. Krupenin, D. E. Presnov, M. N. Savvateev, H. Scherer, A. B. Zorin, and J. Niemeyer, "Noise in Al single electron transistors of stacked design," *J. Appl. Phys.*, vol. 84, pp. 3212–3215, 1998.

[62] D. Vion, A. Aassime, A. Cottet, P. Joyez, H. Pothier, C. Urbina, D. Esteve, and M. H. Devoret, "Manipulating the quantum state of an electrical circuit," *Science*, vol. 296, pp. 886–889, 2002.

[63] J. Koch, T. M. Yu, J. Gambetta, A. A. Houck, D. I. Schuster, J. Majer, A. Blais, M. H. Devoret, S. M. Girvin, and R. J. Schoelkopf, "Charge-insensitive qubit design derived from the Cooper pair box," *Phys. Rev. A*, vol. 76, p. 042319, 2007.

[64] J. A. Schreier, A. A. Houck, J. Koch, D. I. Schuster, B. R. Johnson, J. M. Chow, J. M. Gambetta, J. Majer, L. Frunzio, M. H. Devoret, S. M. Girvin, and R. J. Schoelkopf, "Suppressing charge noise decoherence in superconducting charge qubits," *Phys. Rev. B*, vol. 77, p. 180502, 2008.

[65] A. A. Houck, J. A. Schreier, B. R. Johnson, J. M. Chow, J. Koch, J. M. Gambetta, D. I. Schuster, L. Frunzio, M. H. Devoret, S. M. Girvin, and R. J. Schoelkopf, "Controlling the spontaneous emission of a superconducting transmon qubit," *Phys. Rev. Lett.*, vol. 101, p. 080502, 2008.

[66] F. Yoshihara, K. Harrabi, A. O. Niskanen, Y. Nakamura, and J. S. Tsai, "Decoherence of flux qubits due to $1/f$ flux noise," *Phys. Rev. Lett.*, vol. 97, p. 167001, 2006.

[67] K. Kakuyanagi, T. Meno, S. Saito, H. Nakano, K. Semba, H. Takayanagi, F. Deppe, and A. Shnirman, "Dephasing of a superconducting flux qubit," *Phys. Rev. Lett.*, vol. 98, p. 047004, 2007.

[68] R. C. Bialczak, R. McDermott, M. Ansmann, M. Hofheinz, N. Katz, E. Lucero, M. Neeley, A. D. O'Connell, H. Wang, A. N. Cleland, and J. M. Martinis, "$1/f$ flux noise in Josephson phase qubits," *Phys. Rev. Lett.*, vol. 99, p. 187006, 2007.

[69] F. C. Wellstood, C. Urbina, and J. Clarke, "Low-frequency noise in dc superconducting quantum interference devices below 1 K," *Appl. Phys. Lett.*, vol. 50, pp. 772–774, 1987.

[70] S. Sendelbach, D. Hover, A. Kittel, M. Mück, J. M. Martinis, and R. McDermott, "Magnetism in SQUIDs at millikelvin temperatures," *Phys. Rev. Lett.*, vol. 100, p. 227006, 2008.

[71] T.-C. Wei, D. Pekker, A. Rogachev, A. Bezryadin, and P. M. Goldbart, "Enhancing superconductivity: Magnetic impurities and their quenching by magnetic fields," *Europhys. Lett.*, vol. 75, pp. 943–949, 2006.

[72] A. Rogachev, T.-C. Wei, D. Pekker, A. T. Bollinger, P. M. Goldbart, and A. Bezryadin, "Magnetic-field enhancement of superconductivity in ultranarrow wires," *Phys. Rev. Lett.*, vol. 97, p. 137001, 2006.

[73] R. de Sousa, "Dangling-bond spin relaxation and magnetic $1/f$ noise from the amorphous-semiconductor/oxide interface: Theory," *Phys. Rev. B*, vol. 76, p. 245306, 2007.

[74] L. Faoro and L. B. Ioffe, "Microscopic origin of low-frequency flux noise in Josephson circuits," *Phys. Rev. Lett.*, vol. 100, p. 227005, 2008.

[75] S. Vitale, M. Cerdino, G. A. Prodi, A. Cavalleri, P. Falferi, and A. Maraner, "Linear response and thermal equilibrium noise of magnetic materials at low temperature: Logarithmic relaxation $1/f$ noise, activation, and tunneling," in *Quantum Tunneling of Magnetization – QTM '94*, L. Gunther and B. Barbara, Eds. Norwell, MA: Kluwer, 1995, pp. 157–170.

[76] T. Hime, P. A. Reichardt, B. L. T. Plourde, T. L. Robertson, C. E. Wu, A. V. Ustinov, and J. Clarke, "Solid-state qubits with current-controlled coupling," *Science*, vol. 314, pp. 1427–1429, 2006.

[77] T. Yamamoto, M. Watanabe, J. Q. You, Y. A. Pashkin, O. Astafiev, Y. Nakamura, F. Nori, and J. S. Tsai, "Spectroscopy of superconducting charge qubits coupled by a Josephson inductance," *Phys. Rev. B*, vol. 77, p. 064505, 2008.

[78] M. A. Sillanpää, J. I. Park, and R. W. Simmonds, "Coherent quantum state storage and transfer between two phase qubits via a resonant cavity," *Nature*, vol. 449, pp. 438–442, 2007.

[79] M. Hofheinz, E. M. Weig, M. Ansmann, R. C. Bialczak, E. Lucero, M. Neeley, A. D. O'Connell, H. Wang, J. M. Martinis, and A. N. Cleland, "Generation of Fock states in a superconducting quantum circuit," *Nature*, vol. 454, pp. 310–314, 2008.

Robert McDermott received the Ph.D. degree in physics from the University of California (UC), Berkeley, in 2002. His thesis work involved the development of SQUID-based scanners for nuclear magnetic resonance (NMR) spectroscopy and magnetic resonance imaging (MRI) in microtesla magnetic fields.

From 2003 to 2006, he was a postdoctoral fellow at NIST, Boulder, CO, and UC-Santa Barbara, where he worked to develop high-fidelity Josephson phase qubits. In 2006, he joined the Department of Physics at the University of Wisconsin, Madison. His current research interests include scalable quantum information processing in the solid state, and quantum coherence and entanglement in condensed matter systems.